Stress redistribution in individual ultrathin strained silicon nanowires: a high-resolution polarized Raman study

New Journal of Physics
The open access journal for physics

Stress redistribution in individual ultrathin strained silicon nanowires: a high-resolution polarized Raman study

Alvarado Tarun[1], Norihiko Hayazawa[1,4,5], Maria Vanessa Balois[1,4], Satoshi Kawata[1], Manfred Reiche[2] and Oussama Moutanabbir[1,2,3,5]

[1] Near-field Nanophotonics Research Team, RIKEN, The Institute of Physical and Chemical Research, 2-1 Hirosawa, Wako, Saitama 351-0198, Japan
[2] Max Planck Institute of Microstructure Physics, Weinberg 2, Halle (Saale) D-06120, Germany
[3] Département de Génie Physique, École Polytechnique de Montréal, Montréal, CP 6079, Succursale Centre-Ville, Montréal, Québec H3C 3A7, Canada
[4] Department of Electronic Chemistry, Graduate School of Science and Engineering, Tokyo Institute of Technology, 4259 Nagatsuta, Midori-ku, Yokohama, Kanagawa 2268502, Japan
E-mail: hayazawa@riken.jp and oussama.moutanabbir@polymtl.ca

New Journal of Physics **15** (2013) 053042 (15pp)
Received 7 January 2013
Published 28 May 2013
Online at http://www.njp.org/
doi:10.1088/1367-2630/15/5/053042

Abstract. Strain nano-engineering provides valuable opportunities to create high-performance nanodevices by a precise tailoring of semiconductor band structure. Achieving these enhanced capabilities has sparked a surge of interest in controlling strain on the nanoscale. In this work, the stress behavior in ultrathin strained silicon nanowires directly on oxide is elucidated using background-free, high-resolution polarized Raman spectroscopy. We established a theoretical framework to quantify the stress from Raman shifts taking into account the anisotropy associated with the nanowire quasi-one-dimensional morphology. The investigated nanowires have lateral dimensions of 30, 50 and 80 nm and a length of 1 μm top-down fabricated by patterning and etching 15 nm thick biaxially tensile strained silicon nanomembranes generated using heteroepitaxy

[5] Authors to whom any correspondence should be addressed.

and ultrathin layer transfer. The concern over the contribution of Raman scattering at the nanowire ⟨110⟩ oriented sidewalls is circumvented by precisely selecting the incident polarization relative to the sidewalls of the nanowire, thus enabling an accurate and rigorous analysis of stress profiles in individual nanowires. Unlike suspended nanowires, which become uniaxially strained as a result of free surface-induced relaxation, we demonstrated that stress profiles in single nanowires are rather complex and non-uniform along different directions due to the oxide–nanowire interface. As a general trend, higher stresses are observed at the center of the nanowire and found to decrease linearly as a function of the nanowire width. Using multi-wavelength high-resolution Raman spectroscopy, we also extracted the stress profiles at different depths in the nanowire. The residual stress in the top ∼10 nm of the nanowire was found to be nearly uniaxial and increase from the edge toward the center, which remains highly strained. In contrast, the average stress profiles measured over the whole nanowire thickness exhibit different behavior characterized by a plateau in the region ∼200 nm away from the edges. Our observations indicate that the lattice near the newly formed free surface moves inwards and drags the underlying substrate leading to a complex redistribution of stress. This nanoscale patterning-induced relaxation has direct implications for electrical and mechanical properties of strained silicon nanowires and provides myriad opportunities to create entirely new strained-engineered nanoscale devices.

Contents

1. Introduction

Silicon (Si) nanowires are quasi-one-dimensional nanostructures providing a wealth of opportunities to implement a variety of nanoscale technologies [1–5]. Particularly, nanowire-based architectures have been introduced to extend the lifetime of Si traditional electronics by achieving lower power consumption, higher performance and scalable devices to respond to the relentless course toward the miniaturization imposed by Moore's law [6]. In this perspective, to overcome the limitations faced in the two-dimensional planar devices, transistors with nanowire-like channels are currently used in the fabrication of high-performance microprocessors and memory devices for wireless systems such as mobile phones and radars [6]. Unlike freestanding nanowire-based devices [7], these new technologies employ nanowires having three free facets while the fourth one forms an interface with the underlying substrate [5, 6].

Both of these categories of nanowires suffer, however, from degradation in the carrier velocity as a result of quantum confinement and scattering at the sidewalls, which hinders the device performance [8, 9]. Stress nano-engineering has emerged as a powerful stratagem to alleviate these limitations and extend the capabilities of nanowire-based electronics [7].

Strain engineering has been used in the microelectronics industry since the 90 nm technology node. The main approach currently employed consists of depositing stressor layers on top of transistors. However, as the dimensions of nanowire-based transistors are becoming smaller than the required thickness of such an overlayer, it is difficult to implement this approach into smaller nodes or other nanowire-based architectures. Recently, it was demonstrated that ultrathin, globally strained silicon layers (nanomembranes) are the material of choice to generate strained Si nanowires using top-down nanofabrication processes [7, 10, 11]. Interestingly, upon nanoscale patterning of biaxial strained nanomembranes—a crucial step in the fabrication of strained nanowires—the formation of free surfaces induces a local relaxation of strain due to rearrangement of lattice atoms near the newly formed edges [10, 12–16]. In general, the extent of this phenomenon depends on dimension and geometry [12–16]. However, it is widely admitted that due to nanowire geometry (i.e. the high aspect ratio) the post-patterning stress becomes uniaxial, which means that the stress is fully relaxed along the width of the nanowire [7, 11]. However, as demonstrated in this work, this is not the case for nanowires fabricated directly on oxide. More precisely, the nanowire–substrate interface makes the strain redistribution rather complex as one of the four facets is stabilized by the underlying oxide layer. Exploring and understanding this subtle but important phenomenon is crucial for accurate strain nano-engineering and a precise prediction of the performance of strained Si nanowire-based devices.

In order to accurately probe the evolution of strain in nanoscale, we have developed a method of high-resolution polarized Raman spectroscopy that allows the analysis of the individual contributions of longitudinal-optical (LO) and transverse-optical (TO) phonons and their profiles in a single nanowire [10]. However, the use of a single excitation wavelength (532 nm) in that work can only permit the measurement of phonon profiles averaged over the whole thickness of a nanowire. Moreover, while simultaneous detection of LO and TO phonon modes can directly characterize anisotropic stress relaxations at each position, TO phonon detection is still challenging due to its strong sensitivity to the laser polarization relative to sample geometry and thus the allowed LO phonon is always mixed. Herein, to circumvent these limitations, we employ two excitation wavelengths with linear polarizations corresponding to different penetration depths in silicon, thereby achieving LO phonon detection as a local stress probe at different depths within a single nanowire. We also discuss and take into consideration the effects of the scattering at the nanowire sidewalls on the obtained Raman data and present a method for an accurate determination of stress in nanoscale structures. The effect of the nanowire lateral dimension on the stress relaxation is also addressed.

2. Experimental details

2.1. Sample preparation

The Si nanowires were generated by patterning and etching a 15 nm thick biaxially tensile-strained Si nanomembrane by combining electron beam lithography and dry reactive ion etching. The strained nanomembrane was synthesized by growing epitaxially an ultrathin layer of Si on a ∼500 nm thick $Si_{0.84}Ge_{0.16}$ relaxed buffer layer grown on Si (001) substrate using reduced pressure chemical vapor deposition. The obtained strained-Si/$Si_{0.84}Ge_{0.16}$/Si

heterostructure was subsequently capped by an SiO_2 layer deposited by plasma-enhanced chemical vapor deposition. A second substrate was prepared by deposition of a ~120 nm thick Ge layer on Si (001) using solid-source molecular beam epitaxy. This wafer was also covered by a ~200 nm thick SiO_2 layer. The ultrathin strained Si layer was transferred from the first wafer onto the second one using direct wafer bonding followed by ion-induced slicing and selective chemical etching of SiGe leading to strained $Si/SiO_2/Ge/Si$ heterostructure. The intermediate Ge layer was introduced to prevent the excitation laser from reaching the Si handle substrate in the case of excitation by the laser in the visible range or when the region between nanowires is exposed to the laser. Thus, the background from the underlying Si substrate is eliminated and only the Raman signal from the strained nanowire is detected, thereby achieving a higher sensitivity to local phonons, which is critical for a precise analysis of stress. Ordered arrays of nanowires having a fixed length of 1000 nm and widths of 30, 50 or 80 nm were fabricated. The nanowire arrays were patterned on a negative resist using electron-beam lithography. Reactive ion etching was applied to transfer the pattern to the strained layer. The nanowires are aligned along the $\langle 110 \rangle$ direction and separated by 500 nm from each other to allow the exposure of a single nanowire to the laser beam during Raman analysis. The $\langle 110 \rangle$ nanowires were investigated because of their practical importance as high-performance channels for field effect transistors. The etching was performed at $-60^{\circ}C$ using a mixture of SF_6 (100 sccm) and O_2 (5 sccm) with a relatively low power of 40 W. These conditions were optimized to eliminate possible damage during the etching process. Here the chemical reactivity is dominant. High-resolution transmission electron microscopy investigations (not shown here) confirmed the absence of any damage near the newly formed edges.

2.2. Experimental configuration

Figure 1 displays typical atomic force microscopy (top) and scanning electron microscopy (bottom) images of arrays of nanowires having a width of 80 and 30 nm, respectively. The figure also depicts the sidewalls orientation of the nanowires relative to the polarization of the excitation laser. The long axis of the nanowire is aligned along the $\langle 110 \rangle$ direction. The crystal and the sample coordinate are symbolized as x,y,z and x', y', z', respectively. Porto notation, $z(x'x')z$ or $z(y'y')z$, is used to represent the polarization conditions. The laser beam ($\lambda = 442$ or 355 nm) passes through a linear polarizer and a half-wave plate. The linear polarizer sets the incoming polarization from the laser. The half-wave plate is used to align the incident polarized beam parallel (x') or perpendicular (y') to the nanowire long axis. The beam is then expanded and focused onto the nanowires using an oil-immersion objective lens (numerical aperture = 1.4, $\times 125$). The surface of the strained Si is directly immersed in oil. This configuration improves the laser focusing and minimizes index mismatch-induced spherical aberrations. According to the Rayleigh criterion, the diameter of the laser spot is $\lambda/2$. The backscattered Raman signal is collected by the same objective lens and passes through a pinhole ($\phi = 50\ \mu$m), which leads to an edge filter to block the strong Rayleigh signal in order for the backscattered Raman signal to be detected. The backscattered light goes through an analyzer before reaching a spectrometer (grating = 1800 g mm^{-1}, slit width = 50 μm) equipped with a thermo-electronically cooled charge coupled device (CCD) camera. A single Lorentz function was fitted to the Si Raman peak for all spectra to accurately determine its frequency, width and intensity. The system spectral resolution is 0.02 nm and the accuracy of our analysis after Lorentzian fitting is ~0.02 cm^{-1}. The samples with nanowire arrays were mounted on an x'–y'

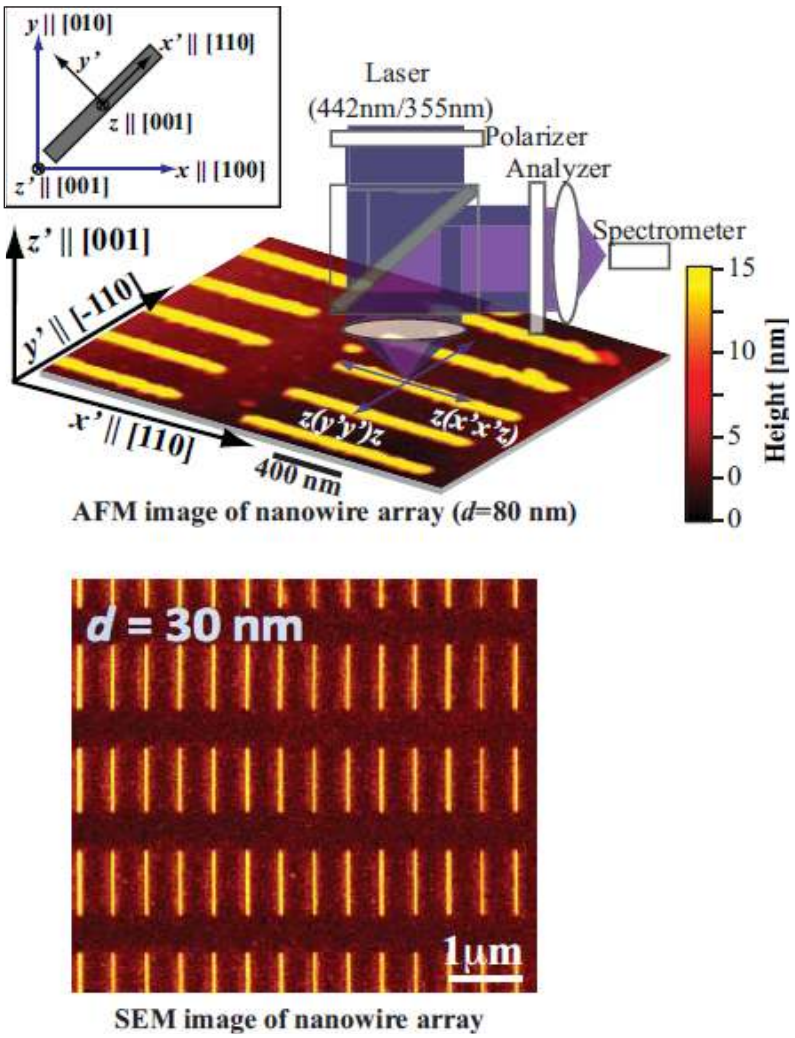

Figure 1. Polarized Raman setup in backscattering configuration showing the AFM image of an array of nanowires with $d = 80$ nm (top). Top view schematic of the nanowire with crystal (x,y,z) and sample (x', y', z') coordinates depicting that the x'- and y'-axes are parallel to the long axis of the nanowire (inset). Shown is the SEM image of an array of nanowires with $d = 30$ nm (bottom).

translation stage and were scanned with a 25 nm step while exposed to the focused laser beam. At each step, a Raman spectrum was recorded. To prevent laser heating, Raman spectra were acquired at 1.0 mW power with a 5 s exposure time using the 442 nm lasers. An exposure of 5 min and a power of 5 μW were used for the 355 nm laser. Note that due to the dependence of the Si absorption coefficient on photon frequency [17], the laser penetration depth $(= \lambda/4\pi k)$ is calculated to be $\sim$10 nm at 355 nm and $\sim$168 nm at 442 nm where λ and k are the wavelength and the imaginary part of the refractive index, respectively. The latter permits probing the stress profiles for the total thickness of the nanowire, whereas the shallower penetration allows the analysis of the top 10 nm of the nanowire.

3. Analytical methods for stress calculation in nanowires

The local stress in the Si lattice is obtained from Raman shifts by solving the well-known secular equation. In the case of the unpatterned nanomembrane, the equi-biaxial ($\sigma_{xx} = \sigma_{yy} = \sigma_0$) model of stress-induced Raman shift for doublet ($\Delta\omega_{xy}$: transverse optical TO phonons) and singlet ($\Delta\omega_z$: longitudinal optical LO phonons) is [18]

$$\Delta\omega_{xy} = [p(S_{11}+S_{12})+q(S_{11}+3S_{12})]\,\sigma_0/2\omega_0 = -3.42\times\sigma_0, \tag{1}$$

$$\Delta\omega_z = [pS_{12}+q(S_{11}+S_{12})]\,(\sigma_{xx}+\sigma_{yy})/2\omega_0 = -4.60\times\sigma_0, \tag{2}$$

where $\Delta\omega_{xy} = \omega_{\varepsilon\text{-Si}} - \omega_{\text{Si}}$ and $\Delta\omega_z = \omega_{\varepsilon\text{-Si}} - \omega_{\text{Si}}$ are expressed in the Raman frequency in each mode in the presence ($\omega_{\varepsilon\text{-Si}}$) and absence ($\omega_{\text{Si}}$) of stress. The $S_{11} = 7.68$ and $S_{12} = -2.14$ (in GPa) are the elastic compliance tensor elements, while $p = -1.85$ and $q = -2.31$ are the phonon deformation potentials for bulk Si at room temperature [19].

The stress relaxation ratio upon patterning at any position in the nanowire is calculated using $R(x, y) = 1 - \sigma_{\text{nanowire}}(x, y)/\sigma_0$, where σ_0 and σ_{nanowire} correspond to the initial stress before nanopatterning and the measured stress in nanowires, respectively [22]. The initial stress, σ_0, in the nanomembrane is calculated from the measured Raman shift using equation (2). However, it is important to note that equation (2) cannot be used for the extraction of stress in nanowires, σ_{nanowire}, mainly because the assumption that shear stress is zero used to obtain the stress is no longer valid as the stress is no longer bi-isotropic in the nanowire due to geometrical constraints and non-uniform rearrangements of atoms near the newly formed free surfaces. In fact, in a nanowire the shearing strain terms at the crystal coordinate are no longer zero due to anisotropic strain relaxation along the nanowire axes. In order to obtain the nanowire stress, we first calculate the strain and stress components in the sample coordinates where shearing terms are all zero due to the symmetry of the structure at the sample coordinate system and then transform them into the crystal coordinate [20]. At the center of the nanowire, the strain component along the nanowire length ($\varepsilon'_{xx}(x', d)$) has almost the value of the original membrane, ε_0, but the stress along the width ($\sigma'_{yy}(x', d)$) will be dramatically relaxed due to the reduced dimension in this direction. d represents the width of nanowires. The shear strain component becomes zero in the middle of the nanowire, and the stress component along z' is equal to zero due to free surface boundary conditions; the strain and stress tensors are then expressed as [20]

$$\{\varepsilon'(x', d)\} = \varepsilon'_{xx}(x', d)\begin{bmatrix} 1 & 0 & 0 \\ 0 & \dfrac{s\alpha(x', d)C_{11}+C_{12}^2-C_{11}(C_{12}-H/2)}{C_{11}(C_{11}+H/2)-C_{12}^2} & 0 \\ 0 & 0 & \dfrac{-s\alpha(x', d)C_{12}-2C_{12}C_{44}}{C_{11}(C_{11}+H/2)-C_{12}^2} \end{bmatrix}, \tag{3}$$

$$\{\sigma'(x', d)\} = \begin{bmatrix} C'_{11}\varepsilon'_{xx}(x', d)+C'_{12}\varepsilon'_{yy}(x', d)+C'_{13}\varepsilon'_{zz}(x', d) & 0 & 0 \\ 0 & \alpha(x', d)\sigma_0 & 0 \\ 0 & 0 & 0 \end{bmatrix}, \tag{4}$$

where $\alpha(x', d) = \sigma'_{yy}(x', d)/\sigma_0$, $s = C_{11}+C_{12}-\left(2C_{12}^2/C_{11}\right)$ and $H = 2C_{44}+C_{12}-C_{11}$. The elastic constants $C_{11} = C_{22} = 166\,\text{GPa}$, $C_{12} = C_{21} = 64\,\text{GPa}$, $C_{44} = 79.6\,\text{GPa}$, $C'_{12} = C_{12} - 0.5H = 35.4\,\text{GPa}$, $C'_{11} = C_{11}+0.5H = 194.6\,\text{GPa}$ and $C'_{13} = C_{12} = 64\,\text{GPa}$ are obtained from [20, 21]. The constant $\alpha(x', d)$ varies between 0 and 1 and depends on the diameter of

the nanowire. At the limits, $\alpha(x', d)$ equals 0 for a uniaxial stress and 1 for a bi-isotropic stress. After substitution, the strain tensor in the sample coordinate reduces to

$$\{\varepsilon'(x', d)\} = \varepsilon'_{xx}(x', d) \begin{bmatrix} 1 & 0 & 0 \\ 0 & 1.06\alpha(x', d) - 0.06 & 0 \\ 0 & 0 & -0.41\alpha(x', d) - 0.36 \end{bmatrix} \quad (5)$$

and after transformation to the crystal coordinate system:

$$\{\varepsilon(x', d)\} = \varepsilon'_{xx}(x', d) \begin{bmatrix} 0.53\alpha(x', d)+0.47 & -0.53\alpha(x', d)+0.53 & 0 \\ -0.53\alpha(x', d)+0.53 & 0.53\alpha(x', d)+0.47 & 0 \\ 0 & 0 & -0.41\alpha(x', d)-0.36 \end{bmatrix}. \quad (6)$$

Using the strain components above, the solution to the well-known secular equation for the LO phonon mode is expressed as

$$\Delta\omega_z = \omega_{\varepsilon\text{-Si}} - \omega_{\text{Si}} = \frac{\omega_{\text{Si}}}{2}[p\varepsilon_{zz}(x', d) + 2q\varepsilon_{yy}(x', d)], \quad (7)$$

$$\Delta\omega_z = \omega_{\varepsilon\text{-Si}} - \omega_{\text{Si}} = \frac{-\omega_{\text{Si}}\varepsilon'_{xx}(x', d)}{2}(1.70\alpha(x', d) + 1.50). \quad (8)$$

In equation (6), there are two unknown parameters, strain $\varepsilon'_{xx}(x', d)$ along the nanowire long x'-axis and $\alpha(x', d)$, the stress relaxation factor along the nanowire width which we have to extract from the Raman measurement. However, assuming we detect only the LO phonon mode by conventional backscattering geometry, it is impossible to determine the two unknown parameters from the single phonon mode. To circumvent this limitation and obtain the stress in nanowires, it is widely accepted that the stress along the width of the nanowire can be assumed to be fully relaxed, that is $\alpha(x', d) = 0$ (see e.g. [13, 20, 21] and references therein). Herein, we demonstrate that this assumption is too simplistic leading to an inaccurate analysis of stress. Using equation (5) and at $\alpha(x', d) = 0$, the stress along the x'-axis is given by $\sigma'_{xx}(x', d) = 169.25 \times \varepsilon'_{xx}(x', d)$. By substituting the strain components in equation (6), $\varepsilon_{zz} = -0.36 \times \varepsilon'_{xx}(x', d)$ and $\varepsilon_{xx} = \varepsilon_{yy} = 0.47 \times \varepsilon'_{xx}(x', d)$, into equation (7), the stress (in GPa) in the long axis can be expressed in terms of the measured Raman shift as

$$\sigma'_{xx}(x', d) = -225.67 \times \frac{\omega_{\varepsilon\text{-Si}} - \omega_{\text{Si}}}{\omega_{\text{Si}}}. \quad (9)$$

In an alternative approach, we propose the introduction of an edge structure (edge parallel to the y'-axis) consisting of a patterned nanomembrane with a practically semi-infinite dimension along y' (>1 cm), which can be assumed as a hypothetical nanowire with an infinite width ($d = \infty$). Equation (8) indicates that there are two unknown parameters, $\varepsilon'_{xx}(x', d)$ and $\alpha(x', d)$, while the experiment only provides the values of $\Delta\omega_z$ (figure 2(b)). For $\alpha(x', d) \neq 0$, $\varepsilon'_{xx}(x', d)$ can be determined using the reference structure ($d = \infty$). Here, the nanowire strain profile along the x'-axis, $\varepsilon'_{xx}(x', d)$, is comparable with the profile along the same direction in the reference structure, $\varepsilon'_{xx}(x', d = \infty) = \varepsilon'_{xx}(x', d)$, because at an identical length (1 μm) the effect of the newly formed free surfaces should be similar in both systems. In the y'-axis, the reference sample is infinite and thus the initial strain is preserved (i.e. no relaxation does take place along this axis), suggesting that $\varepsilon'_{yy}(x', d = \infty)$ is equivalent to the initial strain in the unpatterned nanomembrane, ε_0.

Analogously to equation (8), we introduce an additional anisotropic stress relaxation factor, $\beta(x', d=\infty) = \sigma'_{xx}(x', d=\infty)/\sigma_0$, which represents the relative stress relaxation along the x'-axis in the reference structure. Thus, the equation of Raman shift as a function of $\beta(x', d=\infty)$ can be written as

$$\Delta\omega_z = \omega_{\varepsilon\text{-Si}} - \omega_{\text{Si}} = \frac{-\omega_{\text{Si}}\varepsilon'_{yy}(x', d=\infty)}{2}(1.70\beta(x', d=\infty) + 1.50), \tag{10}$$

where $\varepsilon'_{yy}(x', d=\infty)$ is obtained from the Raman signal of the unpatterned nanomembrane, whereas $\Delta\omega_z$ is obtained from Raman scans along the x'-axis from the edge. By using the obtained values of $\varepsilon'_{yy}(x', d=\infty)$ and $\Delta\omega_z$, we can determine β. Thus, the strain along the x'-axis of the edge sample can be extracted similarly to equation (5) using β:

$$\varepsilon'_{xx}(x', d=\infty) = \varepsilon'_{yy}(x', d=\infty)[1.06\beta(x', d=\infty) - 0.06]. \tag{11}$$

This strain is only a function of x' and varies from $x'=0$ (edge) to an $x'=0.5\,\mu$m around the nanowire center. The strain component, $\varepsilon'_{yy}(x', d=\infty)$ (parallel to the edge), remains unchanged. This approach is analogous to the semi-infinitely wide line structures used in the theoretical treatment developed earlier by Jain *et al* [20]. The measured Raman shifts from the edge structures were attributed mostly to the strain along x', $\varepsilon'_{xx}(x', d=\infty)$, and the constant strain component in the y'-direction, ε_0, which is the same as the strain obtained from the nanomembrane. In the following, we test the validity of these two approaches.

4. Results and discussion

Figure 2(a) shows the Raman spectra obtained with the 442 nm excitation at the center of the nanowires using the $z(x'x')z$ configuration. We reported recently that TO phonons can be effectively observed using high NA illumination [10]. The observed TO-active Raman shifts are upshifted relative to LO phonons as predicted by the association of equations (1) and (2) [10]. This upward shift in the Raman spectra arising from the TO phonon can be easily mixed with the LO phonon signal and consequently overestimates the level of stress relaxation. This is because the spectral split between LO and TO phonons is small to be resolved by peak function fits. Proper selection of sample azimuth, incident polarization and analyzer orientation is therefore necessary to accurately uncover the stress behavior in strained Si nanowires. We observed that the $z(x'x')z$ configuration is constantly lower than the $z(y'y')z$ configuration for all regions in the nanowires. Under $z(x'x')z$, that is the incident polarization is parallel to the nanowire axis, the observed Raman shift is predominantly due to the LO phonon. For the case of $z(y'y')z$, where incident polarization is perpendicular to the nanowire axis, the observed Raman shift consists of both LO and TO phonons [18]. This is because in the $z(y'y')z$ configuration the transverse (E_y) electric field is efficiently converted to the E_z-field when introduced to the (110) and (−110) sidewalls, which results in effective excitation TO phonons [10]. The TO scattered Raman is efficiently collected by backscattering geometry [18]. From our previous work [10], we experimentally verified that TO phonons in nanowires have higher Raman peak shift relative to LO phonons. This explains why the Raman peak shift for $z(y'y')z$ is higher and broader (data not shown) than for $z(x'x')z$. Hence, in order to obtain an accurate in-plane tensile stress from LO phonons, it is important to choose the incident polarization parallel to the nanowire.

Here, the Raman signal is collected from the whole thickness of the nanowire (i.e. 15 nm). The measured spectra are 'background-free' and contain only the intrinsic Si–Si Raman shift peak of the probed nanowire because of the introduction of the Ge interlayer described above.

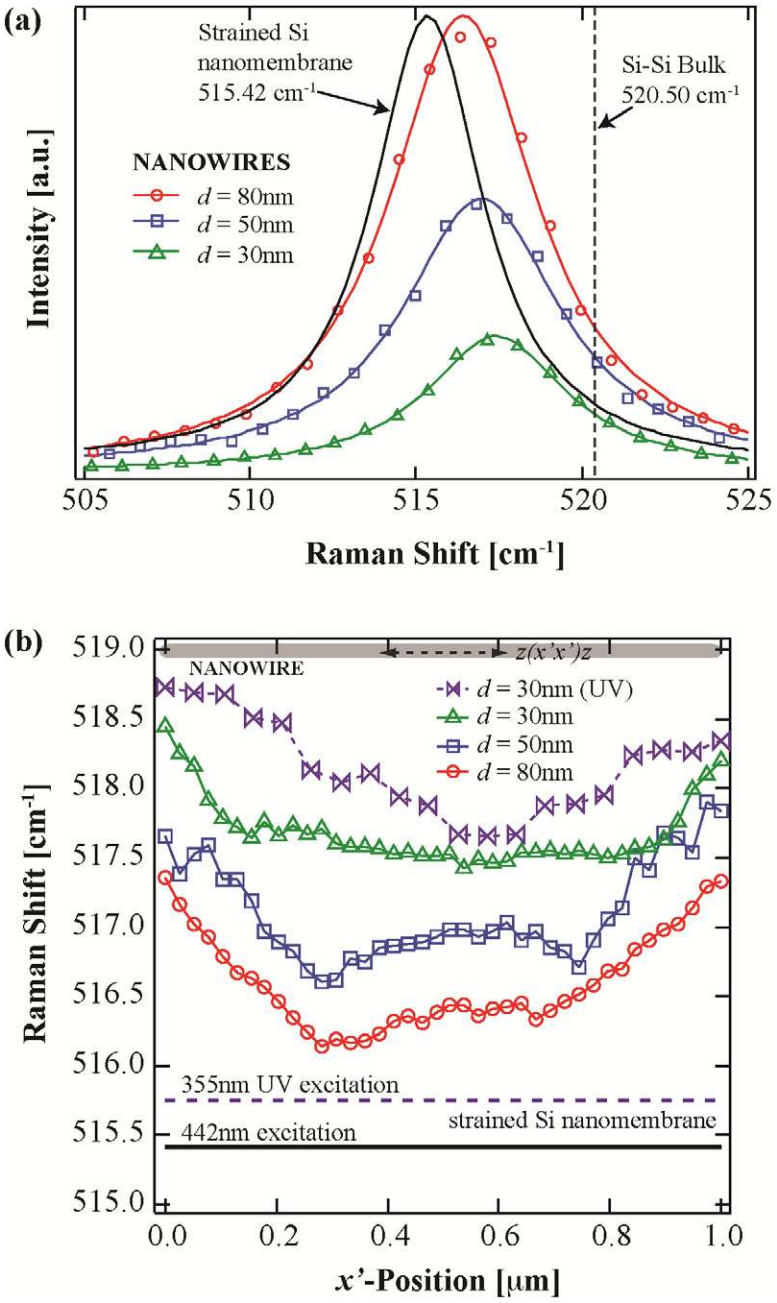

Figure 2. (a) Raman spectra recorded at the center of nanowires with lateral dimensions of 30 nm (triangles), 50 nm (squares) and 80 nm (circles). The Raman spectrum of the unpatterned strained Si is shown in solid black lines. The vertical dashed line denotes the Si–phonon peak position in bulk (unstrained) Si. (b) Profile of the Raman peak for nanowires obtained under the $z(x'x')z$ configuration. The solid and dashed lines represent the Raman peak position of the initial strained Si nanomembrane using the 442 nm (515.42 cm^{-1}) and 355 nm (515.75 cm^{-1}) excitations, respectively. The error bars are smaller than the size of data points.

Table 1. Summary of the Raman peak and spectral width at the center of single nanowires.

Initial strained layer	15 nm thick	($\Delta\omega_z = 515.42\,\mathrm{cm}^{-1}$	$\Delta\upsilon = 4.86\,\mathrm{cm}^{-1}$)
Nanowire width, d (nm)	80	50	30
Peak, $\Delta\omega_z$ (cm^{-1})	516.43	516.99	517.42
Width, $\Delta\upsilon$(cm^{-1})	5.09	5.20	5.16

It should be noted that the dominant contribution to the measured Raman shift originated from the LO phonon mode from both the top (001) surface and the long axis sidewalls, {110}, based on the Raman tensor calculation under x'-polarized light. For the sake of comparison, the Raman spectrum of the initial strained nanomembrane (solid black line) as well as the Si-phonon peak position in bulk Si (broken vertical lines) is shown. Table 1 summarizes the Raman peak and spectral width for all the observed structures. As the width decreases, the Raman peaks shift upward with respect to the position of the Si-phonon peak of the initial strained Si layer.

No significant broadening in the nanowire Si–Si Raman mode is, however, observed. It is noticeable that the Si–Si peak position of the investigated nanowires is upshifted with respect to its position in the initial ($\Delta\omega_z = 515.42\,\mathrm{cm}^{-1}$) strained nanomembrane. This shift is indicative of partial relaxation of stress during the process of nanowire patterning using reactive ion etching.

To obtain more insights into the complex redistribution of stress as nanowire dimension shrinks, the profiles of the Raman shift for nanowires of varying width are plotted in figure 2(b). The nanowires were scanned along the x'-axis with a step size of 25 nm using the $z(x'x')z$ configuration. The Raman shift for $d = 30$ nm using 355 nm (UV) excitation is also displayed in figure 2(b). At this excitation, only the top 10 nm of the nanowire thickness is probed. For comparison, the Raman shifts measured from the original membrane are indicated with solid (442 nm) and dashed (355 nm) lines.

Figure 3 shows the stress profiles using (a) firstly, $\alpha(x', d) = 0$ and (b) secondly, $\varepsilon'_{xx}(x', d) = \varepsilon'_{xx}(x', d = \infty)$ approaches. Regardless of the approaches used, the profiles measured for all the nanowires display qualitatively similar behavior characterized by a more pronounced relaxation of stress near the nanowire edge. Moreover, as a general trend, the residual stress profile shows plateau-like profiles in the region around the center. The breadth of this region is sensitive to the nanowire width and varies from ~400 nm at $d = 50$ or 80 nm to ~700 nm at $d = 30$ nm. The enhanced relaxation near the edges results from the additional free surface as compared to the rest of the nanowires (four versus three facets). As described below, this constant stress value away from the edges can be attributed to the nearly constant and highly retained stress at the buried strained-Si/SiO_2 interface.

The obtained initial stress from the nanomembrane using equation (2) was plotted (solid black) to evaluate the validity of the first approach based on the assumption of a full relaxation along the nanowire width ($\alpha(x', d) = 0$). Strikingly, the stress profile along the long axis obtained using this approach is higher than the original stress in the nanomembrane. This discrepancy indicates that the assumption of a full relaxation along the width is inaccurate and that stress is not uniaxial. In the following, we focus our analysis on the second approach.

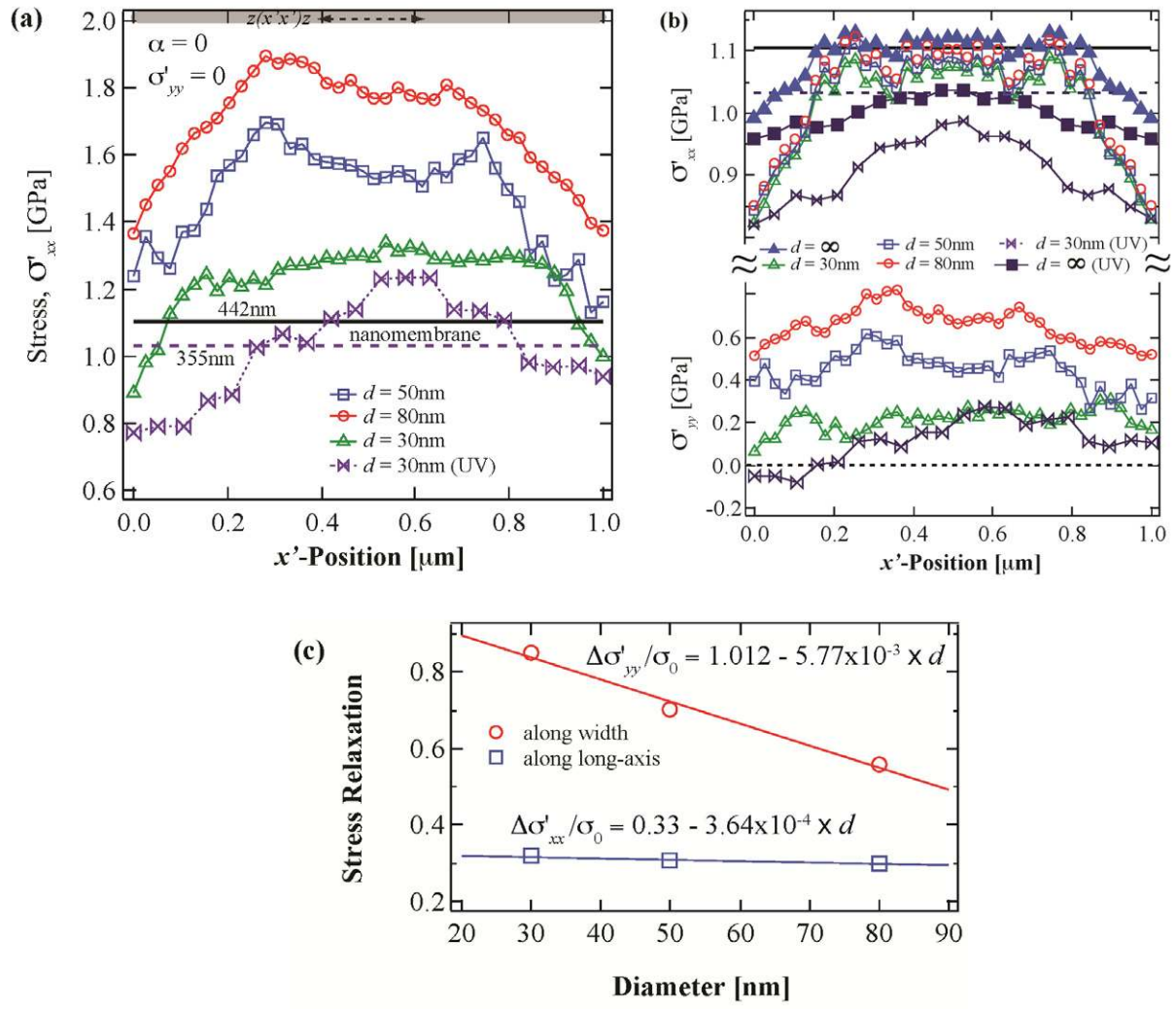

Figure 3. Stress profiles in single nanowires obtained under different excitation wavelengths using the first (a) and second (b) approaches described in the text. (c) Stress relaxation dependence estimated at the center of the nanowire as a function of the nanowire diameter.

We first calculated the strain from equations (10) and (11) using the measured Raman shift scanned from $x' = 0$ (edge) to $x' = 0.5\,\mu$m (towards the center) with semi-infinite width. The strain values are then used in equations (8) and (9) to calculate the stress at each position. Figure 3(b) shows the obtained stress profiles $\sigma'_{xx}(x', d)$ and $\sigma'_{yy}(x', d)$. The calculated stress values along the x'-direction are below the original stress of the membrane. It is also interesting to note that the profile of the stress along the x'-direction of the nanowires is similar and with stress values very close to stress of the edge sample, suggesting that stress is preserved at the center. Moreover, the stress along the x'-direction at the edges ($x' = 0$ and $1.0\,\mu$m) is the same ($\sigma'_{xx}(x', d) \approx 0.85$ GPa) for all nanowires regardless of excitation wavelengths. This is not the case when a full relaxation is assumed along the width, which indicates that this assumption is fraught with large uncertainties. On the other hand, we can clearly see from the profile along the width, $\sigma'_{yy}(x', d)$, that the nanowire is still under a biaxial stress.

The stress profile along the width is relatively constant through the whole length of the nanowire unlike along the long axis where pronounced relaxation is observed at the edges. Furthermore, a full relaxation of stress is only observed at the edge of the nanowire with $d = 30$ nm. For this set of nanowires, the stress at the center reaches a value of ~200 MPa. This behavior is observed for both excitation wavelengths. At $d = 80$ and 50 nm, the stress is well above the fully relaxed region (gray dashed zero line). This result indicates that the overall average stress in the nanowire is biaxial but not bi-isotropic. Note that at an excitation wavelength of 442 nm the buried strained-Si/SiO_2 interface is also probed. Here, the stress between $200 \leqslant x' \leqslant 800$ nm is comparable with the initial stress in the nanomembranes, whereas at 355 nm the initial stress is only preserved in the region $450 \leqslant x' \leqslant 550$ nm. Figure 3(c) exhibits the relaxation ratio at the center of the nanowire as a function of nanowire diameter. It is noticeable that the extent of this relaxation along the width exhibits linear behavior as a function of the nanowire width: $\Delta\sigma'_{yy}/\sigma_0 = 1.01\text{–}5.77 \times 10^{-3} \times d$. The relaxation along the long axis is small and remains unchanged with the nanowire width.

Interestingly, the combination of two excitation wavelengths provides new insights into the complex behavior of stress in nanowires. Figure 4 shows the depth dependence of stress profiles along the two in-plane axes for a nanowire with a width of $d = 30$ nm under the $z(x'x')z$ condition using different excitation wavelengths (penetration depths), namely 442 nm (~168 nm) and 355 nm (~10 nm). It is noteworthy that Raman shifts measured using the 355 nm laser are centered around higher wavenumbers as compared with those obtained using the 442 nm excitation as shown in figure 2(b). Figure 4(a) also displays the original stress (lines) in the unpatterned nanomembrane obtained using the two-excitation wavelengths as well. The small difference in the measured stress using the two excitations suggests that the region near the surface of the nanomembranes is slightly relaxed.

After patterning of the nanowires, the stresses are observed to be more relaxed in both the 442 and 355 nm excitations. However, the interesting observation is that the stress relaxation behavior as obtained by the 355 nm excitation decreases monotonously toward the center of the nanowire, which remains highly strained. At the 442 nm excitation, the stress relaxation plateaus in the region $200 \leqslant x \leqslant 850$ nm. This dissimilarity in stress behavior between the two excitation wavelengths is indicative of the non-uniform distribution of the in-plane stress along the nanowire thickness. More precisely, the fact that the stress measured using a laser with the shallower penetration depth is systematically smaller than the value averaged over the whole thickness provides direct evidence that the region near the nanowire–oxide interface maintains a high level of stress. By combining the stress profiles measured at the 442 nm($\sigma'^{15\,\mathrm{nm}}_{xx}$) and 355 nm $\sigma'^{10\,\mathrm{nm}}_{xx}$ excitations, we extract the stress profile in the bottom 5 nm of the nanowire along the x'-direction σ'^{5nm}_{xx} ($\sigma'^{5\,\mathrm{nm}}_{xx} = 3 \times \sigma'^{15\,\mathrm{nm}}_{xx} - 2 \times (\sigma'^{10\,\mathrm{nm}}_{xx})$) (figure 4(a)). Similarly, the stress profile along the y'-direction is depicted in figure 4(b). For the two in-plane axes, the obtained stress profiles are qualitatively identical but remarkably different from the profiles measured for the top 10 nm or over the whole nanowire thickness. Particularly, the part of the nanowire near the interface is under a higher stress especially in the region about 100–200 nm away from the edge, in qualitative agreement with finite element simulations (not shown). In this region, close stress values are recorded for the two in-plane directions, indicating that the interface with the oxide preserves almost the initial isotropy (i.e. a biaxial strain). Interestingly, the stress in the x'-direction reaches values that are higher than the initial stress, indicating that the contraction of the lattice near the newly formed free surfaces is accompanied by a strong distortion close to the interface with the oxide. This means that when the lattice near the edges moves inwards,

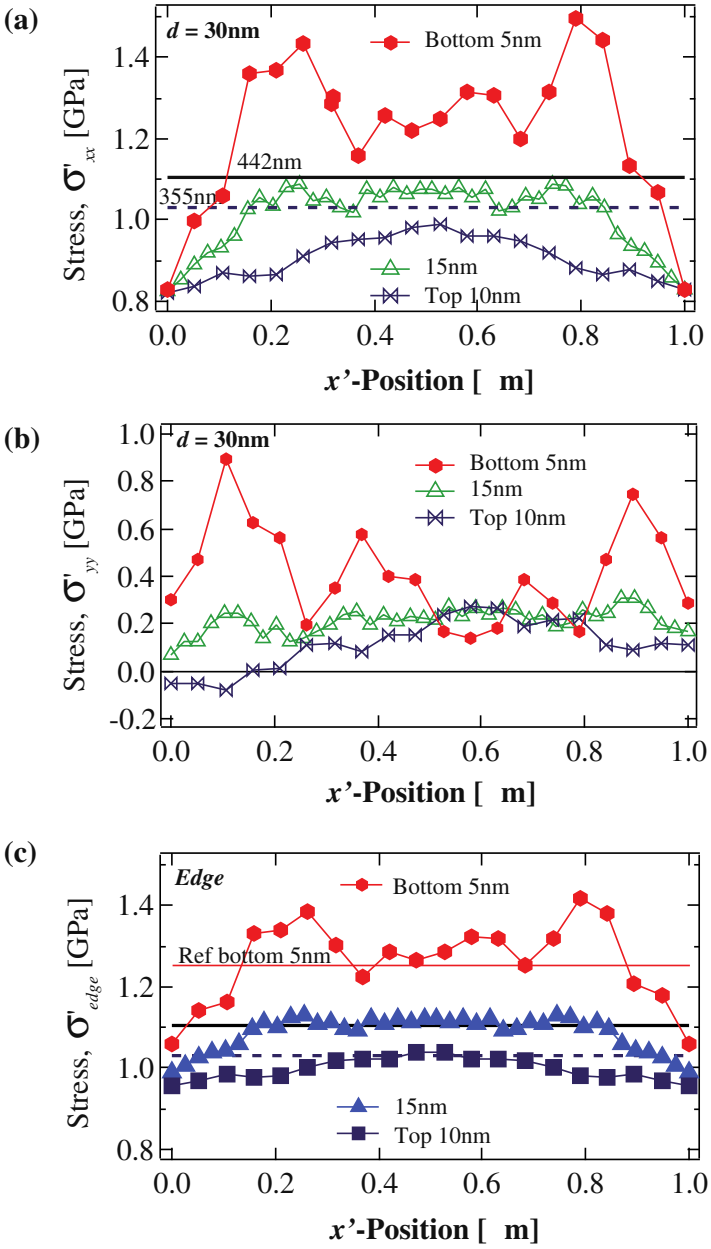

Figure 4. Stress profiles along the (a) x'- and (b) y'-axis for nanowires with a width of $d = 30$ nm at different depths obtained using the two excitation wavelengths (penetration depths): 442 nm (∼168 nm) and 355 nm (∼10 nm). The horizontal solid (442 nm) and dashed (355 nm) lines marked the initial strain in the Si nanomembrane. (c) Stress profiles at different depths in the reference sample with a semi-infinite edge.

it drags the underlying substrate leading to a complex redistribution of stress. Above ∼200 nm away from the edge, the stress decreases slightly along the nanowire length to stabilize around 1.2 GPa. The decrease is more significant along the width. For this direction, the in-plane stress remains the same independently of the depth in the nanowire. Similar behavior is also observed

for the edge sample as shown in figure 4(c). The only noticeable difference in the bottom 5 nm stress values along the long axis between the $d = 30$ nm nanowire and the reference sample is located at the edges. The bottom 5 nm stress at the edge is ~1.06 GPa, which is just above the stress measured with 355 nm excitation whereas for the $d = 30$ nm nanowire, the bottom 5 nm stress is 0.83 GPa. Toward the center, the bottom 5 nm stress values remain unchanged.

5. Conclusion

In summary, we presented a precise method to map the stress in individual strained Si nanowires directly on oxide by using background-free, high-resolution polarized Raman spectroscopy with two excitation wavelengths. We also derived a theoretical framework to extract the stress from Raman shifts, taking into account the stress anisotropy imposed by the nanowire quasi-one-dimensional morphology. We found that adjusting the incident polarization parallel to the long axis of the nanowire is necessary for an accurate Raman probe. Our analysis demonstrates that the assumption of a full relaxation along the shortest dimension is not a valid approximation even for a dimension as small as 30 nm. The obtained stress profiles unraveled the complexity of free surface-induced stress redistribution in patterned nanowires. Besides the anticipated increase in the importance of relaxation for narrower nanowires, the use of two excitation wavelengths provided unprecedented details on the behavior of stress. The obtained stress profiles at different depths clearly demonstrate that the final stress distribution is rather complex, varying from nearly bi-isotropic to uniaxial within the same nanowire. This transition from an initially uniform, isotropic stress to a heterogeneous distribution is the result of a simultaneous contraction of the lattice near the newly formed free surfaces and a tension near the interface with the oxide. The fabrication and design of strained Si nanowire-based devices should take into account this non-uniform distribution of stress. Moreover, these observations provide the basis for more accurate calculations and modeling of stress behavior in nanowires and the associated changes in the physical properties.

Acknowledgments

AT acknowledges the financial support provided by the foreign postdoctoral researcher's (FPR) program in RIKEN. NH gratefully acknowledges financial support from a Grant-in-Aid for Young Scientist (A) No. 21686007 from The Ministry of Education, Culture, Sports, Science and Technology. OM acknowledges funding from NSERC, Canada Research Chair, and École Polytechnique de Montréal (PIED).

References

[1] Yan H, Choe H S, Nam S W, Hu Y, Das S, Klemic J F, Ellenbogen J C and Lieber C M 2011 *Nature* **470** 240
[2] Palacios T 2012 *Nature* **481** 152
[3] Kelzenberg M D, Boettcher S W, Petykiewicz J A, Turner-Evans D B, Putnam M C, Warren E L, Spurgeon J M, Briggs R M, Lewis N S and Atwater H A 2010 *Nature Mater.* **9** 239
[4] Hochbaum A and Yang P 2010 *Chem. Rev.* **110** 527
[5] Colinge J-P *et al* 2010 *Nature Nanotechnol.* **9** 225
[6] Kuhn J K 2011 *Proc. Int. Symp. on VLSI Technology, Systems and Applications (25–27 April 2011)* pp 1–2
[7] Hashemi P, Gomez L and Hoyt J L 2009 *IEEE Electron Device Lett.* **30** 401

[8] Uchida K, Koga J, Ohba R, Numata T and Takagi S-I 2001 *IEDM Technical Digest* 633
[9] Gunawan O, Sekaric L, Majumdar A, Rooks M, Appenzeller J, Sleight J W, Guha S and Haensch W 2008 *Nano Lett.* **8** 1566
[10] Tarun A, Hayazawa N, Ishitobi H, Kawata S, Reiche M and Moutanabbir O 2011 *Nano Lett.* **11** 4780
[11] Minamisawa R A, Süess M J, Spolenak R, Faist J, David C, Gobrecht J, Bourdelle K K and Sigg H 2012 *Nature Commun.* **3** 1096
[12] Moutanabbir O, Reiche M, Hähnel A, Erfurth W, Gösele U, Motohashi M, Tarun A, Hayazawa N and Kawata S 2010 *Nanotechnology* **21** 134013
[13] Ma F, Zhang T-W, Xu K-W and Chu P K 2011 *Appl. Phys. Lett.* **98** 191907
[14] Xiong G, Moutanabbir O, Huang X, Paknejad S A, Shi X, Harder R, Reiche M and Robinson I K 2011 *Appl. Phys. Lett.* **99** 114103
[15] Poborchii V, Tada T, Usuda K and Kanayama T 2011 *Appl. Phys. Lett.* **99** 191911
[16] Moutanabbir O, Reiche M, Hähnel A, Oehme M and Kasper E 2010 *Appl. Phys. Lett.* **97** 053105
[17] Palik E D 1985 *Handbook of Optical Constants of Solids* (San Diego, CA: Academic)
[18] De Wolf I 1996 *Semicond. Sci. Technol.* **11** 139
[19] Miyatake T and Pezzotti G 2011 *J. Appl. Phys.* **110** 093511
[20] Jain S C, Dietrich B, Richter H, Atkinson A and Harker A H 1995 *Phys. Rev.* B **52** 6247
[21] Chandrasekhar M, Renucci J B and Cardona M 1978 *Phys. Rev.* B **17** 1623
[22] Moutanabbir O, Reiche M, Hähnel A, Erfurth W, Gösele U, Motohashi M, Tarun A, Hayazawa N and Kawata S 2010 *Appl. Phys. Lett.* **96** 233105